nature photonics

ARTICLES

https://doi.org/10.1038/s41566-020-0677-y

Sub-nanometre resolution in single-molecule photoluminescence imaging

Ben Yang[1,4], Gong Chen[1,4], Atif Ghafoor[1], Yufan Zhang[1], Yao Zhang[1], Yang Zhang[1]✉, Yi Luo[1], Jinlong Yang[1], Vahid Sandoghdar[2], Javier Aizpurua[3], Zhenchao Dong[1]✉ and J. G. Hou[1]✉

Ambitions to reach atomic resolution with light have been a major force in shaping nano-optics, whereby a central challenge is achieving highly localized optical fields. A promising approach employs plasmonic nanoantennas, but fluorescence quenching in the vicinity of metallic structures often imposes a strict limit on the attainable spatial resolution, and previous studies have reached only 8 nm resolution in fluorescence mapping. Here, we demonstrate spatially and spectrally resolved photoluminescence imaging of a single phthalocyanine molecule coupled to nanocavity plasmons in a tunnelling junction with a spatial resolution down to ~8 Å and locally map the molecular exciton energy and linewidth at sub-molecular resolution. This remarkable resolution is achieved through an exquisite nanocavity control, including tip-apex engineering with an atomistic protrusion, quenching management through emitter–metal decoupling and sub-nanometre positioning precision. Our findings provide new routes to optical imaging, spectroscopy and engineering of light–matter interactions at sub-nanometre scales.

The advent of scanning near-field optical microscopy (SNOM) ignited great hopes for reaching atomic resolution using photons[1–13], an idea that was considered unreachable due to the Abbe limit[11]. Nevertheless, atomic resolution in SNOM has proven to be elusive. In a nutshell, the resolution in near-field microscopy depends on the degree of optical field confinement[8,14–20], which is very quickly lost as the probe's size and its separation to the sample are increased[11,19,21]. Recently, ångström scale spatial resolution was successfully demonstrated in tip-enhanced Raman spectroscopy (TERS) of a single molecule on metal surfaces[22–24]. In this arrangement, a nanocavity plasmon (NCP) field is confined down to the sub-nanometre scale[25,26] in a scanning tunnelling microscope (STM) junction. However, unlike the light-scattering process in TERS, photoluminescence (PL) imaging with similar resolution has not been realized because fluorescence is expected to be strongly quenched in the very immediate vicinity of metals[6,7,15,27–29].

Parallel to the efforts in near-field imaging, research on plasmonic nanocavity antennas has shown that light emission can be enhanced by orders of magnitudes for an emitter sandwiched between a plasmonic nanoparticle and a metallic surface[30–41]. In this case, the physics can be described by the enhancement of the photonic density of states (PDOS) due to the electromagnetic boundaries of a confined region, as known from cavity quantum electrodynamics[42]. At the nanometre scale, the modification of PDOS is expected to be dictated by atomic-scale features[26], but direct laboratory investigations of this and related phenomena have not been accessible by existing near-field optical measurements. To this end, it would be highly desirable to tailor the optical properties of quantum emitters by engineering their atomic-scale external boundaries and drive the spatial resolution down to sub-nanometre scales in optically excited near-field microscopy.

In this work, through the precise junction control over both the Ag tip apex with an atomistic protrusion and the molecular electronic states decoupled from a silver substrate, we demonstrate NCP-enhanced PL imaging from a single zinc phthalocyanine (ZnPc) molecule with sub-nanometre resolution. The exquisite control of cryogenic ultrahigh-vacuum STM in three dimensions with sub-nanometre precision also enables quantitative analyses on the dependence of the field confinement and fluorescence enhancement as a function of gap distances, which, together with theoretical simulations, unravels the crucial elements for achieving such a high resolution and provides insights into the photophysical mechanism on the ever-increasing fluorescence enhancement when the tip approaches to the molecule. Moreover, by exploiting sub-nanometre-resolved PL spectroscopic imaging, we also map the spatial distribution of spectral densities such as peak energies and linewidths, probing and manipulating subtle plasmon–molecule interactions at the sub-molecular scale.

Results and discussion

Figure 1a illustrates the strategy we used to achieve fluorescence from a single zinc phthalocyanine (ZnPc) molecule in an STM junction with the tip-enhanced PL (TEPL) technique, which is illustrated in Extended Data Fig. 1 (see Methods for experimental details). Here we combined electronic decoupling of the molecular emitter from the plasmon-active metal substrate with strongly localized plasmonic enhancement via tip-apex engineering with an atomistic protrusion. A three-monolayer-thick sodium chloride (NaCl) dielectric spacer was used as an effective decoupling layer to suppress molecular fluorescence quenching due to the direct electron transfer between the ZnPc molecules and the Ag(100) substrate[36,43]. In order to provide strong NCP enhancement for PL, electrochemically etched silver tips were first treated by ion bombarding and annealing to form a smooth surface, which was followed by controlled gentle tip indentations to the Ag(100) substrate to create an atomistic protrusion at the tip apex (detailed in Supplementary Section 1). Such a tip structure, when approaching a silver substrate, is believed to be capable of confining laser-generated

[1]Hefei National Laboratory for Physical Sciences at the Microscale and Synergetic Innovation Centre of Quantum Information and Quantum Physics, University of Science and Technology of China, Hefei, China. [2]Max Planck Institute for the Science of Light, Erlangen, Germany. [3]Materials Physics Centre CSIC-UPV/EHU and Donostia International Physics Centre DIPC, Donostia-San Sebastián, Spain. [4]These authors contributed equally: Ben Yang, Gong Chen. ✉e-mail: zhyangnano@ustc.edu.cn; zcdong@ustc.edu.cn; jghou@ustc.edu.cn

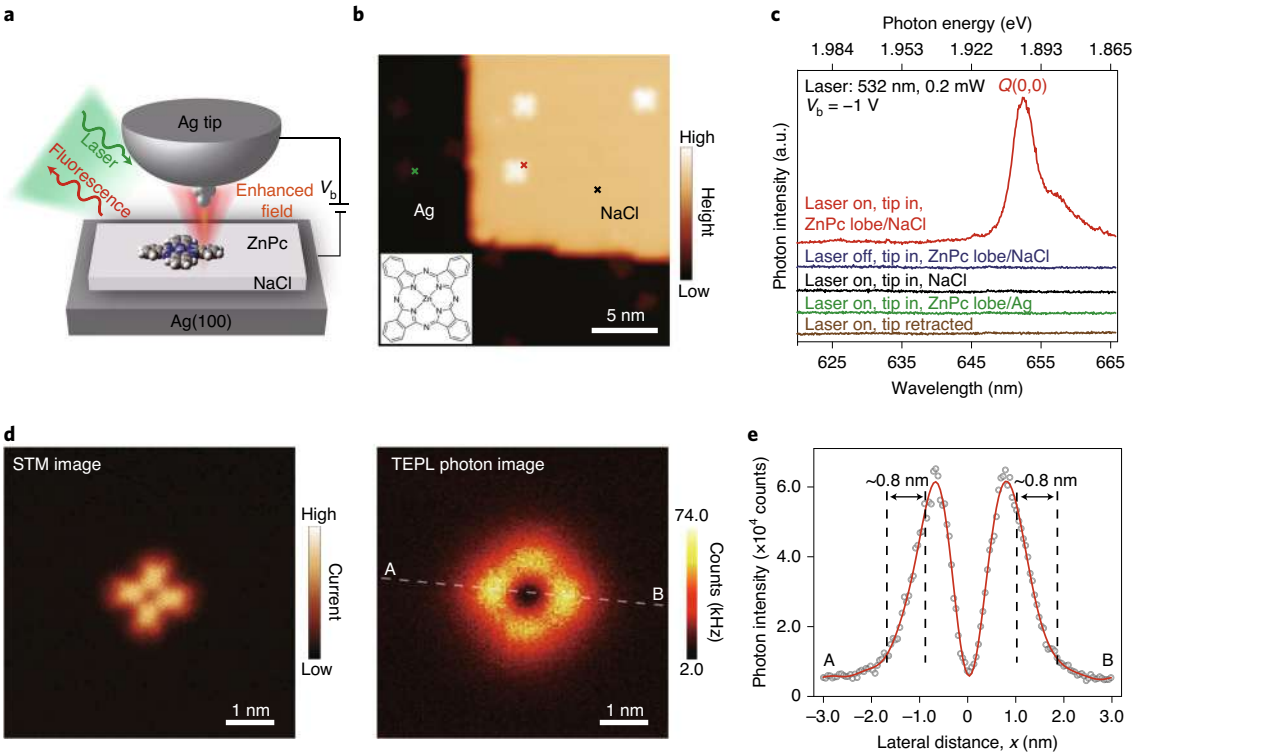

Fig. 1 | Sub-nanometre-resolved single-molecule TEPL imaging. a, Schematic of the experimental set-up for generating NCP-enhanced PL from a single ZnPc molecule on three-monolayer-thick NaCl/Ag(100), highlighting the role of the atomistic protrusion at the Ag tip apex in producing highly confined electromagnetic fields. V_b, bias voltage. **b**, STM image showing isolated ZnPc molecules on a three-monolayer-thick NaCl island and bare Ag(100) surface (taken at −1 V, 2 pA). The inset shows the molecular structure of ZnPc. The central Zn atom is located above a chlorine atom with the diagonal lobes oriented along the [011] surface direction. **c**, TEPL spectra (532 nm, 0.2 mW, 120 s; −1 V, 2 pA) acquired at different positions marked with coloured crosses in **b**. For comparison, a laser-off spectrum (blue) and a tip-retracted spectrum (brown) are also displayed. The spectra are offset for clarity. *Q* refers to the electronic transition from the first excited singlet S_1 state to the ground state S_0. **d**, Simultaneously recorded STM image (left) and TEPL photon image (right) of a single ZnPc molecule on three-monolayer-thick NaCl/Ag(100) in the constant-height mode. The photon image was collected by a single-photon avalanche diode (SPAD) with a bandpass filter (655 nm ± 7.5 nm). **e**, Photon intensity profile for the dashed white line A–B in the photon image in **d**. Grey open circles, raw experimental data; red line, smoothed curve; dashed vertical lines, markers for the lateral distances corresponding to 10% or 90% in the PL intensity contrast.

plasmonic fields into a very small volume at the very end of the tip apex[26], which not only locally excites a decoupled single molecule efficiently, but also dramatically enhances its photon emission rate to the far field. The engineered Ag tip is also able to provide high-resolution STM imaging, as exemplified in Fig. 1b, showing isolated ZnPc molecules adsorbed on a three-monolayer-thick NaCl island and bare Ag(100) surface, respectively. The four-lobe feature observed for each molecule is in good agreement with its molecular structure shown in the inset.

Of particular interest is the different light emission behaviours shown in Fig. 1c for different laser conditions (on or off) and tip positions (for example, above a molecule or away from it). When the incident laser (532 nm) is on and the tip is positioned above the lobe of a single ZnPc molecule on the three-monolayer-thick NaCl surface (marked with a red cross in Fig. 1b), we observe a clear molecule-specific emission band at ~653 nm that is associated with the *Q*(0,0) transition of the ZnPc molecule[36]. The molecular excitation process here is believed to be purely optical by incident photons because the molecule-specific emission disappears completely when the laser is turned off (blue curve in Fig. 1c). The energy of tunnelling electrons at an applied bias voltage of −1 V is much smaller than the optical bandgap of ZnPc molecules ($E_{gap} \approx 1.90$ eV) and is thus not sufficient to excite the electronic transition of the ZnPc molecule. The molecular PL signal here (red curve in Fig. 1c) is also found to originate from only the particular single ZnPc molecule underneath the tip, as the emission spectrum is featureless when the tip is positioned above the nearby bare three-monolayer-thick NaCl surface (marked with a black cross in Fig. 1b), which also confirms that the tip is contamination-free. It should be borne in mind that the photoluminescence of ZnPc molecules deposited directly on the bare Ag surface is quenched completely due to the electronic hybridization between the molecule and metal (green curve in Fig. 1c).

The realization of clear single-molecule TEPL presented above (red curve of Fig. 1c) indicates the validity of the combined strategy adopted, which allows us to overcome fluorescence quenching even though the tip–molecule distance is so small: below 1 nm under the tunnelling condition of −1 V and 2 pA. Moreover, it also implies a large fluorescence enhancement, demonstrated by the sharp contrast in the absence of molecule-specific emission when the tip is fully retracted (brown curve in Fig. 1c). According to the coverage of ZnPc molecules on three-monolayer-thick NaCl islands and the spot size of the focusing laser beam on the sample, there are millions of ZnPc molecules under illumination on the surface (Supplementary Section 2). But without the tip, their fluorescence is still quenched by the underlying metal substrate. The approaching tip is thus the unambiguous cause of the enhancement of the fluorescence signal. A conservative estimation of the enhancement factor[28] is on the order of ~10^8 with respect to the tip-free situation

(detailed in Supplementary Section 2). Such a large enhancement factor suggests that the tip–substrate nanocavity serves as a highly efficient optical antenna for generating a strong and confined plasmonic field, thus boosting plasmonic enhancement for both excitation and emission of a single ZnPc molecule. In this sense, the fluorescence of molecules close to the Ag substrate is 'rescued' by the large radiative yield generated by the NCP-induced local density of electromagnetic states.

Such a strong and confined plasmonic field also allows us to probe the optical response within a single molecule. As shown in Fig. 1d, the photon image for the $Q(0,0)$ band emission of a single ZnPc molecule exhibits a ring-like pattern with four emission maxima at the lobes and a dark feature at the centre. Such a pattern has two implications. First, it directly reveals the existence of two equivalent transition dipoles oriented horizontally and in orthogonal orientations. The dark centre is associated with the dipole symmetry of the whole system. The NCP–molecule coupling for the horizontally oriented transition dipole tends to cancel out when the tip is above the molecular centre[36,44]. Second, the clear observation of the four-bright-maxima pattern, rather than a nearly perfect ring-like pattern, suggests that the point–dipole model fails[45]. To describe the experimental imaging pattern, the spatial distribution of the electronic transition density (that is, the real chemical structure of a molecule) should be taken into account. On the basis of the optical contrast through the 10–90% flank[36] of the photon emission intensity across a molecule (Fig. 1e), the spatial resolution of the TEPL imaging is estimated to be ~0.8 nm, reaching the sub-nanometre scale.

The sub-nanometre resolution in the single-molecule TEPL photon image correlates closely with the spatial confinement of the local plasmonic field. To explore the nature of the tip structure that can produce such a highly confined plasmonic field, we investigate its dependence on the gap distance. This is made possible by the remarkable capability of STM under ultrahigh-vacuum and low-temperature (7 K) conditions to precisely control and measure both the lateral (x) and vertical (d) distances between the tip and molecule (Fig. 2a, see details in Supplementary Section 3). As shown in Fig. 2b for the lateral line-trace TEPL spectra at six different gap distances, the molecular emissions become weaker and less confined with increasing gap distances. Such an evolution is more clearly illustrated in Fig. 2c, with two evident features. First, the PL intensity drops rapidly with increasing gap distances due to the decreased strength of the plasmonic field. An exponential fit to the normalized PL intensity reveals a highly sensitive gap-distance dependence of the NCP field with a very small decay length of ~0.17 nm (Fig. 2d).

The second feature in Fig. 2c is the slower emission decay across a molecule with increasing d, which implies a less confined plasmonic field in the lateral direction for larger d. In the present work, the lateral confinement of the plasmonic field (w) is estimated via the spatial resolution of TEPL according to the 10%–90% optical contrast for the emission evolution shown in Fig. 2c for each d. Thus, by fitting the w–d plot using the widely adopted formula for NCP $w \approx \sqrt{Rd}$ (refs. [21,46,47]), an effective tip radius (R) of ~0.5 nm can be obtained for the tip apex (Fig. 2e). Considering that the typical radius of an electrochemical etched Ag tip in our experiments is around 50 nm (ref. [28]) and that the radius of a Ag atom is ~0.15 nm, such a small tip radius indicates that there is an atomistic protrusion composed of a few Ag atoms at the apex of the tip, which can further concentrate the NCP field down to the sub-nanometre scale through an atomic-scale lightning rod effect[26,45]. As expected for the highly sensitive gap-distance dependence of the NCP field associated with such an atomistic tip protrusion, the single-molecule TEPL photon imaging (as shown in Fig. 2f) quickly becomes blurred with a small increase in d, which occurs in parallel with the spectral evolution observed in Fig. 2b and is also supported by theoretical simulations (detailed in Supplementary Section 4).

The precise control of the tip positions demonstrated in Fig. 2 also enables us to further investigate the intriguing photophysics of molecular fluorescence enhancement and quenching at the STM cavity when the tip gradually approaches the molecule and finally makes a contact, as schematically illustrated in Fig. 3a. The TEPL intensity is found to first increase and then decrease sharply to zero when the tip is brought closer to the molecule gradually (Fig. 3b, see Supplementary Section 5 for the estimation of the tip–molecule distance). Such a process can be divided into three regimes of interactions based on the correlations between the TEPL intensity and the tip–molecule distance as well as on the evolution of the tunnelling current recorded (Fig. 3a,b). In regime I, the tip approaches the molecule but does not make contact, the peak intensity and spectral linewidth of the molecular emission are found to continue increasing. In regime II, the fluorescence signal starts to fall, as the molecule can jump to the tip owing to stronger tip–molecule interactions as the tip gets closer to the molecule. The ZnPc molecule inside the junction in this case is likely to switch between two configurations: either tilted with one lobe attached to the tip or lying flat on the NaCl surface, as implied by the oscillations of tunnelling currents due to two different conductance states[48]. When the molecule is attached to the tip, the direct electron transfer between the tip and the ZnPc would quench the fluorescence signal; but when the molecule is off the tip, the fluorescence signal recovers, thus leading to the sharp drop in the mixed TEPL intensities in regime II as the tip gets closer and closer. In regime III, as the tip–molecule distance decreases further, the tip finally contacts the molecule firmly, resulting in complete quenching without any molecular fluorescence.

Of particular interest is the intriguing photophysics revealed in regime I, in which the molecular fluorescence is found to keep increasing until the tip makes contact with the molecule. This behaviour is very different from previous reports for isolated plasmonic nanostructures where the molecular fluorescence is quenched for an emitter–metal separation of less than 5 nm (refs. [6,7,27]). This is due to the formation of a plasmonic nanocavity, which dramatically enhances the emitter's excitation and radiative decay rate, as proposed in the literature[30,31,33,34]. However, for the present situation with the molecular transition dipole oriented horizontally on the NaCl surface, the observed behaviour of fluorescence enhancement is found to also rely on the presence of an atomistic protrusion at the tip apex, in addition to the important role of the NCP. According to our theoretical simulations (detailed in Supplementary Section 6), for a tip with a radius of 50 nm but without an atomistic protrusion, the fluorescence intensity tends to decrease at small tip–molecule distances when the tip approaches a ZnPc emitter above the Ag substrate. By contrast, for a tip with an atomistic protrusion, when the tip approaches very close to a ZnPc molecule, a strong and highly localized NCP field is generated between the Ag substrate and the atomistic protrusion of the Ag tip, which provides a very large plasmonic enhancement to the radiative decay rate and resultant quantum efficiency, owing to the additional atomic-scale lightning rod effect (Fig. 3c,d). Equally important is the generation of substantial lateral field components around the atomistic protrusion, which can effectively excite the horizontally oriented transition dipole of a ZnPc molecule in close proximity. Such massive enhancement of the excitation and radiative decay rate leads to both the monotonous increase in the TEPL intensity for very short tip–molecule distances and the fluorescence enhancement by about seven orders of magnitude relative to the tip-free situation (Fig. 3d). We note that the use of a plasmon-active metal substrate such as Ag is important for generating strong fluorescence enhancement. Calculated fluorescence intensities are much weaker by four orders of magnitude if a dielectric substrate (for example, NaCl or glass) is used instead, even when using a Ag tip with an atomistic protrusion. In other

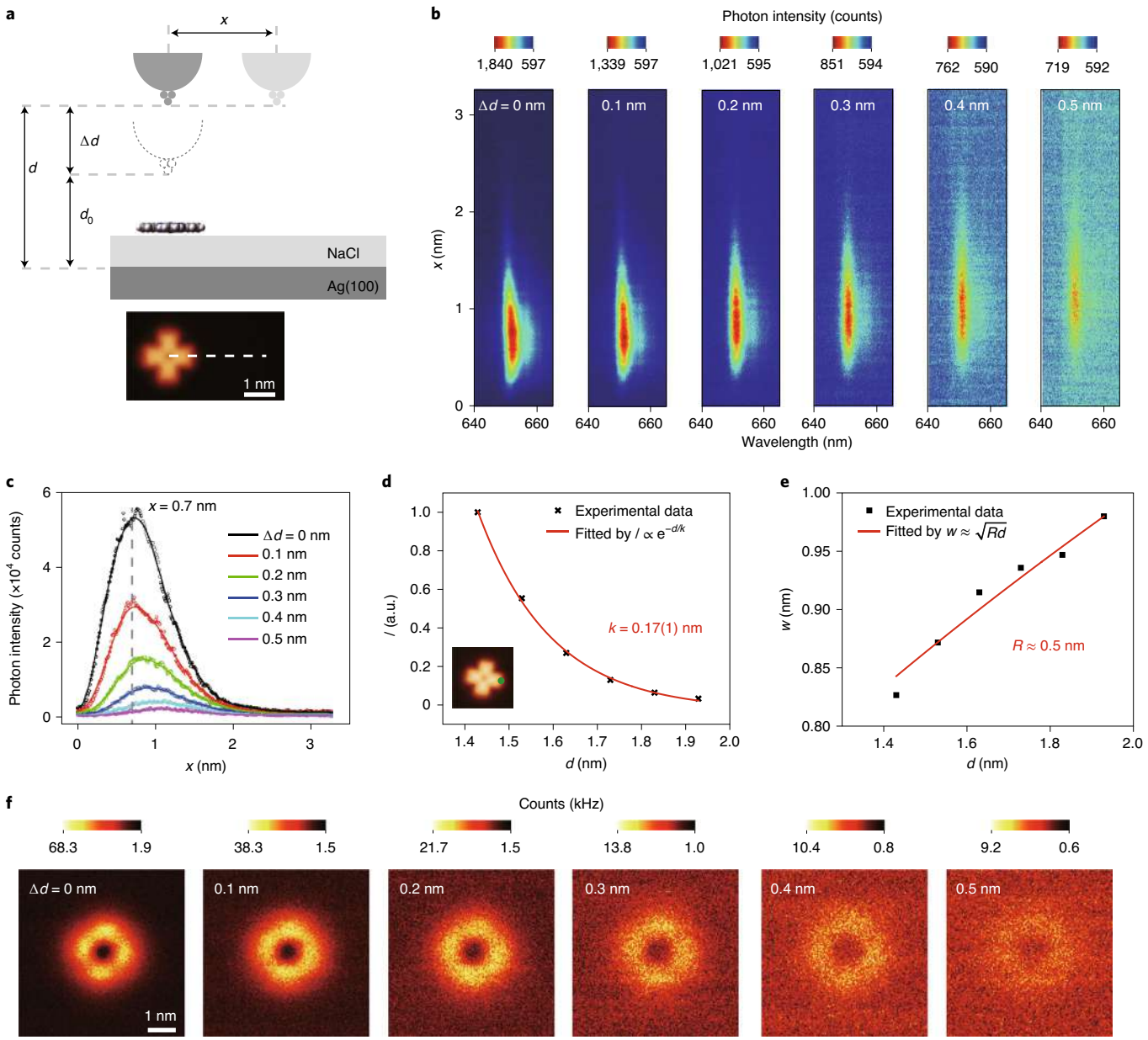

Fig. 2 | Evolution of spatial resolution for photon images at different gap distances. a, Top: schematic of the junction geometrical parameters. d_0 is the initial gap distance and Δd the increment of the gap distance. Bottom: STM image illustrating the line trace for the lateral displacement. **b**, Spectral evolution of TEPL for the line trace shown in **a** (integration time per spectrum: 3 s; step size: 11 pm; total steps: 300) for $\Delta d = 0$–0.5 nm from left to right. **c**, TEPL intensities (integrated over 653 nm ± 2.5 nm for each spectrum in **b**) plotted as a function of x for the six different gap distances. The background signal has been subtracted. Open circles, raw experimental data; solid lines, smoothed curves. **d**, Gap-distance dependence of normalized TEPL intensities (I) extracted from **c** along the dashed vertical line. The green point in the inset, which is 0.7 nm away from the centre, marks the position where the spectra were collected. k is the decay constant from an exponential fit, with the standard deviation shown in parentheses. **e**, Plasmonic field confinement plotted against the gap distance. **f**, Gap-distance-dependent photon images acquired in the constant-height mode by a SPAD with a bandpass filter (655 nm ± 7.5 nm).

words, for an NCP-free nanocavity, the molecular fluorescence is quenched. In this sense, for the present system, quenching is suppressed as a result of both the presence of an atomistic protrusion at the tip apex and the large local density of electromagnetic states associated with the NCP between the tip and metal substrate.

The sub-nanometre-resolved PL imaging ability demonstrated above offers an opportunity to investigate subtle plasmon–molecule interactions at the sub-molecular scale[45] (Supplementary Section 7). Figure 4a–d shows results of spatially and spectrally resolved PL spectroscopic imaging over a single ZnPc molecule. For a molecule in a plasmonic nanocavity, its transition dipole experiences the electromagnetic interaction from its own field; that is, the field acts back on the molecule after being scattered by the nanocavity[29,43,49,50]. Such self-interaction can result in the optical dressing of molecular excited states and thus lead to tip-position-dependent modifications of the transition energy and decay rate. As shown in Fig. 4b, clear differences can be observed in the peak intensities, energies and linewidths of the PL spectra measured at five different positions. The strongest molecular emission intensity is obtained when the tip is positioned above the

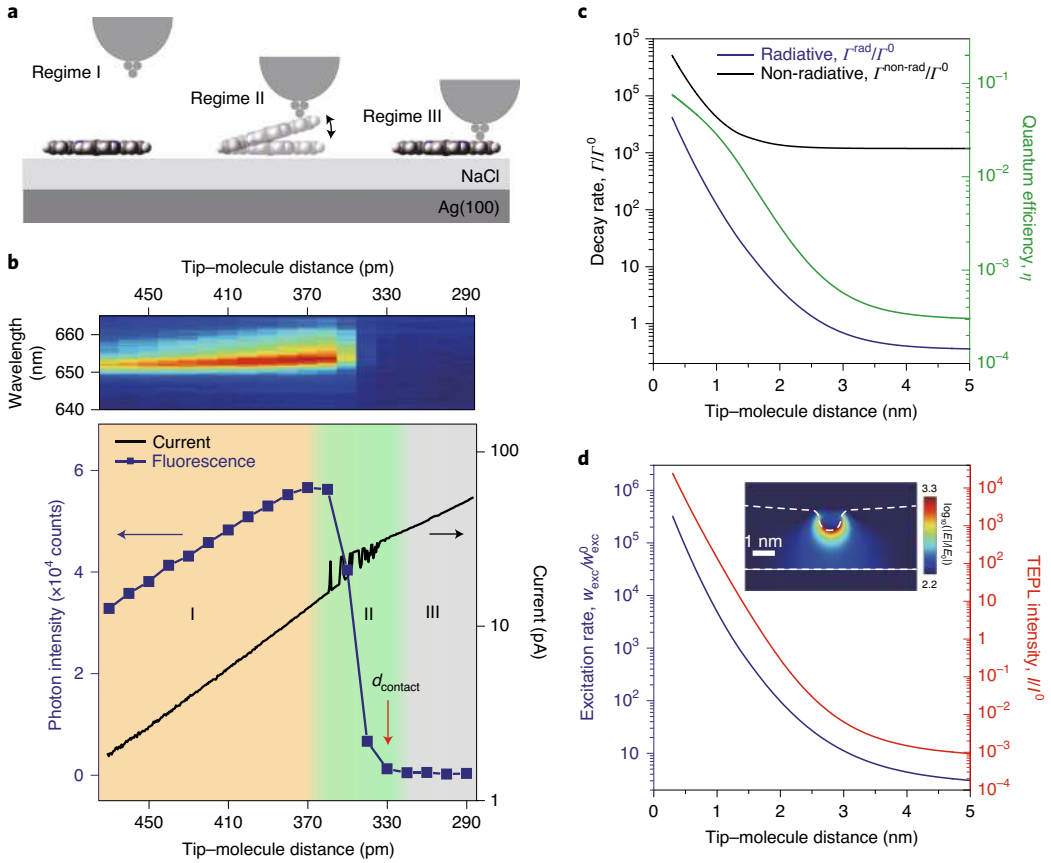

Fig. 3 | Revealing the photophysics of ZnPc in a plasmonic nanocavity by tracking the evolution of TEPL intensities at different tip–molecule distances. **a**, Schematic showing three different tip–molecule distance regimes in TEPL. **b**, Top: waterfall plot of TEPL spectra for different tip–molecule distances (initial set-point condition: −0.7 V, 2 pA; vertical step distance: 10 pm; integration time per spectrum: 1 s). Bottom: gap-distance-dependent PL intensities (blue curve) (integrated over 653 nm ± 2.5 nm) after subtracting the background signal. The measured change in the tunnelling current when the tip gradually approaches the molecule is shown with the black line. The red arrow marks the distance for a firm tip–molecule contact ($d_{contact}$). **c**, Simulated radiative and non-radiative decay rates and quantum efficiency at different tip–molecule distances. Γ is the radiative or non-radiative decay rate of the ZnPc molecule in the plasmonic nanocavity. **d**, Simulated excitation rate and TEPL intensity at different tip–molecule distances. Inset: simulation of the total field enhancement ($|E/E_0|$) distribution inside the gap. In **c** and **d**, the value plotted for each physical quantity is normalized with the corresponding free-space value.

lobe, with the peak energy strongly redshifted and the peak linewidth considerably broadened. Such spectral shifts and linewidth broadenings are mainly caused by plasmon–molecule interactions (Supplementary Section 6). Theoretically, the spectral shift ($\Delta\omega$) and linewidth broadening ($\Delta\Gamma$) are directly associated with the real and imaginary part of the molecular self-interaction induced by the plasmonic nanocavity, described by $\Delta\omega \propto -\mathrm{Re}\left[\boldsymbol{\mu}_0^* \cdot \mathbf{E}_{\mathrm{scat}}(\mathbf{r}, \boldsymbol{\omega_0})\right]$ and $\Delta\Gamma \propto \mathrm{Im}\left[\boldsymbol{\mu}_0^* \cdot \mathbf{E}_{\mathrm{scat}}(\mathbf{r}, \boldsymbol{\omega_0})\right]$, respectively. Here $\boldsymbol{\mu}_0$ is the molecular transition dipole moment, $\mathbf{E}_{\mathrm{scat}}(\mathbf{r}, \omega_0)$ is the local field that acts back at the molecule at position $\mathbf{r}$ after scattered by the nanocavity and ω_0 is the energy of the molecule in free space. The former ($\Delta\omega$) is also known as the photonic Lamb shift[29,43,49,50], and usually causes the emission energy to shift to red in a plasmonic nanocavity; the latter quantity ($\Delta\Gamma$) is associated with the decay rate, which is usually enhanced by the Purcell effect due to the change in the PDOS[30,49,50].

The delicate influence of such a self-interaction on the spatial distribution of spectral densities within a single molecule is best illustrated in the panoramic view of the peak energy and linewidth maps in Fig. 4c,d. Both reveal a four-lobe pattern with sub-molecular resolution. When the tip is positioned above the ZnPc lobes, the emission band peaks at ~1.901 eV, but above the gap positions between ZnPc lobes, it peaks at ~1.903 eV. Although the separation between these two positions is only ~0.6 nm, the difference in the amount of spectral redshift is as high as 2 meV, which strongly suggests a change in the local electromagnetic environment at the sub-nanometre scale. The redshift becomes smaller and smaller as the tip moves away from the molecule, yielding a pronounced change of ~7 meV in the photonic Lamb shift across a molecule. In contrast to the sharp changes in the peak energy, the four-lobe pattern is relatively vague for the linewidth map (Fig. 4d). This can be understood by the relatively small change in the decay rate across a molecule and the challenge in precisely measuring the small variations of the linewidths. The observed linewidth of about 8–11 meV for the $Q(0,0)$ peak in the TEPL spectra is mainly composed of the contributions from the molecular self-interaction induced by the plasmonic nanocavity (5.7–8.7 meV) and the dephasing (~2.3 meV) (see Supplementary Section 7 for more details). The experimental pattern of spatially resolved peak shifts and linewidths within a single molecule can be qualitatively reproduced by the electromagnetic simulations based on both a tip apex with an atomistic protrusion and a real ZnPc chemical structure (Supplementary Section 6), as shown in Fig. 4e,f. Such agreement, together with the spectral variations observed within a molecule, indicates that the molecular self-interaction in a plasmonic nanocavity (or plasmon–molecule interaction) is highly

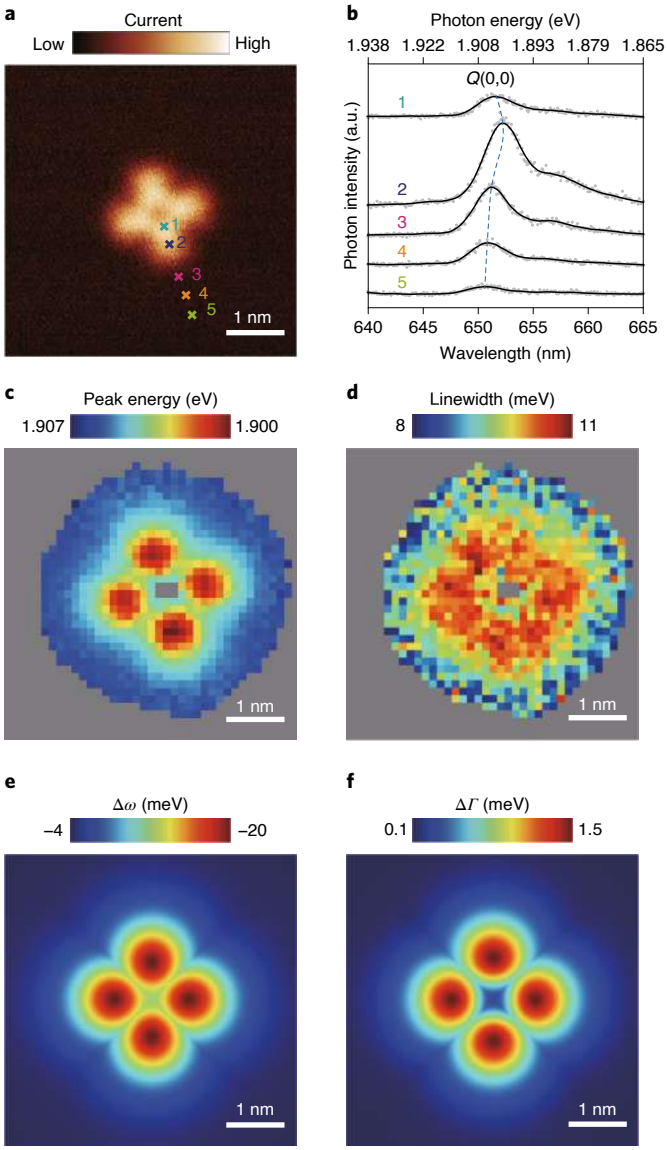

Fig. 4 | Revealing subtle plasmon–molecule interactions at the sub-molecular level by spectroscopic imaging. a, STM image of a single ZnPc molecule on three-monolayer-thick NaCl/Ag(100). **b**, Representative PL spectra acquired at different molecular positions marked with crosses in **a**. The spectra are shifted vertically for clarity. **c**,**d**, Peak energy (**c**) and linewidth (**d**) maps obtained from the experimental spectroscopic image, which was acquired for the same area in **a** (5 nm × 5 nm, 40 pixels × 40 pixels, 2 s per pixel). **e**,**f**, Simulated maps of the peak shift (**e**) and linewidth broadening (**f**) induced by the plasmonic nanocavity with an atomistic protrusion. The STM image, PL spectra and spectroscopic images were acquired in the constant-height mode, with the height regulated at the set-point tunnelling condition of −1 V and 2 pA on the ZnPc lobe.

sensitive to the local electromagnetic environment, specifically to the relative arrangement of the molecular transition dipole with respect to the atomic-scale NCP field (including separation and orientation). The TEPL spectroscopic imaging we demonstrate here provides the ability to access such interaction at the sub-nanometre scale.

Conclusion

In conclusion, we have demonstrated sub-nanometre-resolved single-molecule near-field photoluminescence imaging and spectroscopy. Three key elements have been identified as contributing to this achievement: (1) the tip should be plasmon-active with an atomistic protrusion on the tip apex; (2) the single molecule should be electronically decoupled from a plasmonic substrate through a dielectric spacer of atomic-scale thickness; and (3) the junction geometry should be precisely controlled in three dimensions with sub-nanometre precision. Together, these conditions allow us to generate a strong and highly confined NCP field for the massive excitation and emission enhancement of a single molecule, establishing that to achieve a resolution down to the sub-nanometre scale in SNOM, both the size of the tip and its distance to the emitter must be on the same scale. With such a junction design and control, the molecular fluorescence is found to exhibit a monotonically enhancing behaviour, rather than becoming quenched, as the tip approaches the molecule to the point of contact. The approach we demonstrated here not only allows luminescent species to be imaged, but also provides direct optical information about their interactions with the local photonic environment, both at sub-nanometre resolution. Our findings can also be generalized to non-scanning architectures, where molecules and nanostructures with atomic features are carefully nanofabricated, thus paving the way for engineering light–matter interactions at the sub-molecular level.

Online content

Any methods, additional references, Nature Research reporting summaries, source data, extended data, supplementary information, acknowledgements, peer review information; details of author contributions and competing interests; and statements of data and code availability are available at https://doi.org/10.1038/s41566-020-0677-y.

Received: 30 April 2020; Accepted: 9 July 2020;
Published online: 10 August 2020

References

1. Lewis, A., Isaacson, M., Muray, A. & Harootunian, A. Scanning optical spectral microscopy with 500 Å spatial resolution. *Biophys. J.* **41**, 405a (1983).
2. Pohl, D. W., Denk, W. & Lanz, M. Optical stethoscopy: image recording with resolution λ/20. *Appl. Phys. Lett.* **44**, 651–653 (1984).
3. Betzig, E. & Chichester, R. J. Single molecules observed by near-field scanning optical microscopy. *Science* **262**, 1422–1425 (1993).
4. Michaelis, J., Hettich, C., Mlynek, J. & Sandoghdar, V. Optical microscopy using a single-molecule light source. *Nature* **405**, 325–328 (2000).
5. Frey, H. G., Witt, S., Felderer, K. & Guckenberger, R. High-resolution imaging of single fluorescent molecules with the optical near-field of a metal tip. *Phys. Rev. Lett.* **93**, 200801 (2004).
6. Anger, P., Bharadwaj, P. & Novotny, L. Enhancement and quenching of single-molecule fluorescence. *Phys. Rev. Lett.* **96**, 113002 (2006).
7. Kühn, S., Håkanson, U., Rogobete, L. & Sandoghdar, V. Enhancement of single-molecule fluorescence using a gold nanoparticle as an optical nanoantenna. *Phys. Rev. Lett.* **97**, 017402 (2006).
8. Ma, Z., Gerton, J. M., Wade, L. A. & Quake, S. R. Fluorescence near-field microscopy of DNA at sub-10 nm resolution. *Phys. Rev. Lett.* **97**, 260801 (2006).
9. Höppener, C., Lapin, Z. J., Bharadwaj, P. & Novotny, L. Self-similar gold-nanoparticle antennas for a cascaded enhancement of the optical field. *Phys. Rev. Lett.* **109**, 017402 (2012).
10. Mauser, N. & Hartschuh, A. Tip-enhanced near-field optical microscopy. *Chem. Soc. Rev.* **43**, 1248–1262 (2014).
11. Weisenburger, S. & Sandoghdar, V. Light microscopy: an ongoing contemporary revolution. *Contemp. Phys.* **56**, 123–143 (2015).
12. Hermann, R. J. & Gordon, M. J. Nanoscale optical microscopy and spectroscopy using near-field probes. *Annu. Rev. Chem. Biomol. Eng.* **9**, 365–387 (2018).
13. Park, K.-D., Jiang, T., Clark, G., Xu, X. & Raschke, M. B. Radiative control of dark excitons at room temperature by nano-optical antenna-tip Purcell effect. *Nat. Nanotechnol.* **13**, 59–64 (2018).
14. Gerton, J. M., Wade, L. A., Lessard, G. A., Ma, Z. & Quake, S. R. Tip-enhanced fluorescence microscopy at 10 nanometer resolution. *Phys. Rev. Lett.* **93**, 180801 (2004).
15. Agio, M. & Alù, A. *Optical Antennas* (Cambridge Univ. Press, 2013).
16. Matsuzaki, K. et al. Strong plasmonic enhancement of biexciton emission: controlled coupling of a single quantum dot to a gold nanocone antenna. *Sci. Rep.* **7**, 42307 (2017).

17. Chikkaraddy, R. et al. Mapping nanoscale hotspots with single-molecule emitters assembled into plasmonic nanocavities using DNA origami. *Nano Lett.* **18**, 405–411 (2018).
18. Groß, H., Hamm, J. M., Tufarelli, T., Hess, O. & Hecht, B. Near-field strong coupling of single quantum dots. *Sci. Adv.* **4**, eaar4906 (2018).
19. Chen, X. et al. Modern scattering-type scanning near-field optical microscopy for advanced material research. *Adv. Mater.* **31**, 1804774 (2019).
20. Park, K.-D. et al. Tip-enhanced strong coupling spectroscopy, imaging, and control of a single quantum emitter. *Sci. Adv.* **5**, eaav5931 (2019).
21. Becker, S. F. et al. Gap-plasmon-enhanced nanofocusing near-field microscopy. *ACS Photon.* **3**, 223–232 (2016).
22. Zhang, R. et al. Chemical mapping of a single molecule by plasmon-enhanced Raman scattering. *Nature* **498**, 82–86 (2013).
23. Lee, J., Crampton, K. T., Tallarida, N. & Apkarian, V. A. Visualizing vibrational normal modes of a single molecule with atomically confined light. *Nature* **568**, 78–82 (2019).
24. Zhang, Y. et al. Visually constructing the chemical structure of a single molecule by scanning Raman picoscopy. *Natl Sci. Rev.* **6**, 1169–1175 (2019).
25. Benz, F. et al. Single-molecule optomechanics in "picocavities". *Science* **354**, 726–729 (2016).
26. Barbry, M. et al. Atomistic near-field nanoplasmonics: reaching atomic-scale resolution in nanooptics. *Nano Lett.* **15**, 3410–3419 (2015).
27. Dulkeith, E. et al. Fluorescence quenching of dye molecules near gold nanoparticles: radiative and nonradiative effects. *Phys. Rev. Lett.* **89**, 203002 (2002).
28. Huang, Y. P. et al. Shell-isolated tip-enhanced Raman and fluorescence spectroscopy. *Angew. Chem.* **130**, 7645–7649 (2018).
29. Zhang, F. L. et al. Elucidating molecule–plasmon interactions in nanocavities with 2 nm spatial resolution and at the single-molecule level. *Angew. Chem.* **131**, 12261–12265 (2019).
30. Kinkhabwala, A. et al. Large single-molecule fluorescence enhancements produced by a bowtie nanoantenna. *Nat. Photon.* **3**, 654–657 (2009).
31. Russell, K. J., Liu, T.-L., Cui, S. & Hu, E. L. Large spontaneous emission enhancement in plasmonic nanocavities. *Nat. Photon.* **6**, 459–462 (2012).
32. Belacel, C. et al. Controlling spontaneous emission with plasmonic optical patch antennas. *Nano Lett.* **13**, 1516–1521 (2013).
33. Faggiani, R. M., Yang, J. & Lalanne, P. Quenching, plasmonic, and radiative decays in nanogap emitting devices. *ACS Photon.* **2**, 1739–1744 (2015).
34. Kongsuwan, N. et al. Suppressed quenching and strong-coupling of purcell-enhanced single-molecule emission in plasmonic nanocavities. *ACS Photon.* **5**, 186–191 (2018).
35. Qiu, X., Nazin, G. & Ho, W. Vibrationally resolved fluorescence excited with submolecular precision. *Science* **299**, 542–546 (2003).
36. Zhang, Y. et al. Visualizing coherent intermolecular dipole–dipole coupling in real space. *Nature* **531**, 623–627 (2016).
37. Imada, H. et al. Real-space investigation of energy transfer in heterogeneous molecular dimers. *Nature* **538**, 364–367 (2016).
38. Kuhnke, K., Grosse, C., Merino, P. & Kern, K. Atomic-scale imaging and spectroscopy of electroluminescence at molecular interfaces. *Chem. Rev.* **117**, 5174–5222 (2017).
39. Doppagne, B. et al. Electrofluorochromism at the single-molecule level. *Science* **361**, 251–255 (2018).
40. Kimura, K. et al. Selective triplet exciton formation in a single molecule. *Nature* **570**, 210–213 (2019).
41. Doppagne, B. et al. Single-molecule tautomerization tracking through space-and time-resolved fluorescence spectroscopy. *Nat. Nanotechnol.* **15**, 207–211 (2020).
42. Haroche, S. & Raimond, J.-M. *Exploring The Quantum: Atoms, Cavities, and Photons* (Oxford Univ. Press, 2006).
43. Zhang, Y. et al. Sub-nanometre control of the coherent interaction between a single molecule and a plasmonic nanocavity. *Nat. Commun.* **8**, 15225 (2017).
44. Chen, C., Chu, P., Bobisch, C., Mills, D. & Ho, W. Viewing the interior of a single molecule: vibronically resolved photon imaging at submolecular resolution. *Phys. Rev. Lett.* **105**, 217402 (2010).
45. Neuman, T. S., Esteban, R., Casanova, D., García-Vidal, F. J. & Aizpurua, J. Coupling of molecular emitters and plasmonic cavities beyond the point-dipole approximation. *Nano Lett.* **18**, 2358–2364 (2018).
46. Rendell, R. & Scalapino, D. Surface plasmons confined by microstructures on tunnel junctions. *Phys. Rev. B* **24**, 3276–3294 (1981).
47. Savage, K. J. et al. Revealing the quantum regime in tunnelling plasmonics. *Nature* **491**, 574–577 (2012).
48. Schmaus, S. et al. Giant magnetoresistance through a single molecule. *Nat. Nanotechnol.* **6**, 185–189 (2011).
49. Kalkbrenner, T. et al. Optical microscopy via spectral modifications of a nanoantenna. *Phys. Rev. Lett.* **95**, 200801 (2005).
50. Novotny, L. & Hecht, B. *Principles of Nano-Optics* (Cambridge Univ. Press, 2012).

Methods

Our STM imaging and TEPL experiments were performed on a custom-built optical–STM system operating under ultrahigh vacuum (~5.0×10^{-11} torr) and at liquid helium cryogenic conditions (~7 K), as shown in Extended Data Fig. 1. The Ag(100) substrate used in the present work was cleaned by cycles of argon ion sputtering and annealing. Ag tips were used in all of our experiments (see Supplementary Section 1 for detailed information on the tip fabrication). ZnPc molecules were thermally evaporated onto the Ag(100) surface, partially covered by NaCl islands, at liquid helium conditions. To remove the possible influence of the tip trajectory on spectroscopic imaging, all PL photon images and spectroscopic images presented in this work were measured in the constant-height mode[51]. Bias voltages were applied to the sample. The tunnelling conditions were chosen specifically to provide precise control of junction geometries (such as the tip–molecule distance), but not to electrically excite the molecule directly.

A single-longitude-mode diode-pumped laser at 532 nm (CrystaLaser, CL532-100-SO) was used to provide a linearly polarized laser beam (>300:1) for PL excitation. The beam was fibre-coupled to a dark box via a single-mode polarization-maintaining fibre with a collimated output beam diameter of ~1.0 mm, passing through a half waveplate to achieve desired p-polarization. A round continuously variable metallic neutral density filter (ND filter) was used to adjust the laser output power. Two reflective mirrors were used to provide freedom for optical alignment. The laser beam is reflected by a 30:70 (reflection:transmission) beam splitter into ultrahigh vacuum through a quartz viewport. The collimated beam was refocused by an aspheric lens (back focal length $f_b = 12.4$ mm, numerical aperture NA = 0.46) on the tip–substrate junction at an angle of 60° from the surface normal. The diameter of the laser spot on the sample surface at the optimal focus was ~30 μm. The PL signal was collected through the same lens, filtered to remove residual laser light by a 532 nm long-pass edge filter and then fibre-coupled to a spectrometer using a slit size of ~100 μm. The PL signal was dispersed by a 600 grooves per mm grating and detected by a liquid-nitrogen-cooled CCD (charge-coupled-device). Another beam splitter was used to help align the excitation and collection optical paths, which are removed from the optical path when collecting the PL signal. The laser power used in the PL experiments presented in this work was kept at 0.2 mW. The TEPL spectroscopic imaging was carried out through a synchronization function between the STM controller and CCD camera at each pixel during scanning, acquiring a PL spectrum at each pixel. We also used a SPAD detector to map the PL intensity signal filtered by a bandpass filter (655 nm ± 7.5 nm), by simultaneously recording the photon signal at each pixel during scanning through an external auxiliary channel in the STM controller. All PL spectra presented here were not corrected for the wavelength dependent sensitivity of photon detection systems.

In Fig. 1d, the photon image was acquired with normal STM scan conditions and thus has a relatively high pixel resolution and scan speed (128 pixels × 128 pixels, 5 ms per pixel). In Fig. 2a, the lateral tip displacement (x) is defined from the molecular centre to the outside along the lobe direction. The initial gap distance (d_0) is defined by the set-point tunnelling condition of −1 V and 2 pA above the molecular centre. The increment of the gap distance (Δd) was realized through the vertical tip motion after switching off the feedback loop. In Fig. 3c,d, a full quantum chemistry description of the degenerated molecular dipoles is adopted, namely by considering the spatial distribution of transition densities of the ZnPc chemical structure. The same model is also used for theoretical simulations presented in Fig. 4. In our data processing of Fig. 4, the values of peak energies and linewidths for the $Q(0,0)$ transition were obtained through a double-Lorentzian fitting to account for the asymmetric lineprofile with a weak vibronic shoulder around 658 nm.

Data availability

The data that support the findings of this study are available from the corresponding authors on reasonable request.

Code availability

The MATLAB codes used for the electromagnetic calculations in this study are available from the corresponding authors on reasonable request.

References

51. Hecht, B., Bielefeldt, H., Inouye, Y., Pohl, D. & Novotny, L. Facts and artifacts in near-field optical microscopy. *J. Appl. Phys.* **81**, 2492–2498 (1997).

Acknowledgements

We thank B. Wang for helpful discussions. This work was supported by the National Key R&D Program of China (grant numbers 2016YFA0200600 and 2017YFA0303500), the National Natural Science Foundation of China, the Strategic Priority Research Program of the Chinese Academy of Sciences (grant number XDB36000000) and the Anhui Initiative in Quantum Information Technologies. J.A. acknowledges project IT1164-19 of the consolidated university groups from the Basque Government.

Author contributions

Z.D. and J.G.H. conceived and supervised the project. B.Y., A.G., Yufan Zhang and Yang Zhang performed experiments and analysed data. G.C. and Yao Zhang derived the theory and performed theoretical simulations. B.Y., G.C., Yao Zhang, Yang Zhang, Y.L., J.Y., V.S., J.A., Z.D. and J.G.H contributed to the data interpretation. Z.D., B.Y., G.C., Yang Zhang, J.A., V.S. and J.G.H. co-wrote the manuscript. All authors discussed the results and commented on the manuscript.

Competing interests

The authors declare no competing interests.

Additional information

Extended data is available for this paper at https://doi.org/10.1038/s41566-020-0677-y.

Supplementary information is available for this paper at https://doi.org/10.1038/s41566-020-0677-y.

Correspondence and requests for materials should be addressed to Y.Z., Z.D. or J.G.H.

Reprints and permissions information is available at www.nature.com/reprints.

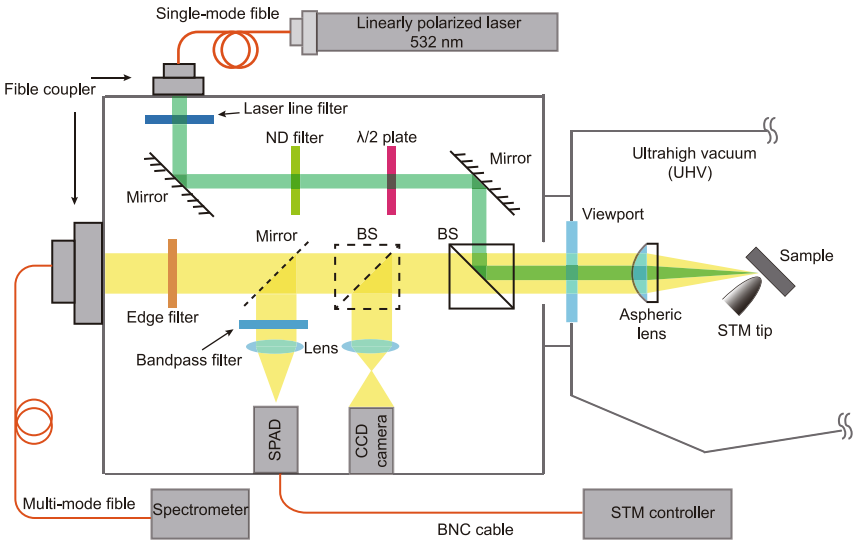

Extended Data Fig. 1 | Schematic drawing of our custom-built experimental setup for TEPL measurements. This setup is composed of four sub-systems: a laser source for light excitation, a dark-box for optical filtering, polarization control and alignment, a low-temperature UHV STM for sample preparation and characterization with a built-in lens for both light excitation and collection, and a photon detection sub-system containing a SPAD for PL intensity measurements and a spectrometer equipped with a highly sensitive CCD detector for PL spectral measurements.